Deformation of Polymers (A survey of polymer crystallization by X-ray diffraction . chapter 7)

Chapter 7. Deformation of Polymers

7.1 Introduction

Mechanical deformation was widely studied in the polymer morphology. Various models were proposed for the mechanisms of semi-crystalline substances by drawing, rolling etc. [1-15]. Peterlin *et al.* performed precise investigations on the deformation process of polymers, which involve rotation of lamellae, chain tilt and slip, destruction of lamellae before yielding, and formation of a new structure after yielding. On the deformation procedures, there is a fundamental problem not yet clearly explained, whether the original lamellae are partly destroyed and immediately incorporated into the deformed texture, or whether they are once completely melted and recrystallized into the oriented texture.

The materials hitherto investigated were various polymers, especially polyethylene, in the forms of unoriented bulk material, two-dimensional (thin) spherulite, oriented film (by drawing or rolling), blown film, single crystal. In these investigations, there was no change in the crystalline structure before and after the deformation. However, if there is a sample, which never crystallizes again into the same crystal lattice after destruction, it may be useful to investigate the above problem. The β-phase material of isotactic polypropylene (β-PP) consistently satisfies the above requirement by the following properties:

Firstly, when the β-crystal (hexagonal lattice) is destroyed or melted, molecules are not recrystallized into the β-form but transformed into the α–crystal (monoclinic lattice), which is thermally stable and has a melting temperature 10 °C higher than the former one. In the α-crystal, helical molecules are incorporated in the right- and left-handed helices alternately, whereas in the β-crystal, all helices are the same [16,17]. As a result, the phase transition between these crystals needs the rewinding of helices and cannot take place without local unfolding or melting and subsequent recrystallization. When the β→α phase transition occurs during the deformation, which can be detected easily by the distinct WAXS patterns, the original β-crystal is destroyed by melting or unfolding of the original texture and recrystallized into the α-crystal.

Secondly, this sample has unidirectional lamellar orientation as a result of TSC with the lamellar long axis parallel to the growth direction (See in chapter 5). This is of great advantage in interpreting the X-ray patterns because of the crystalline orientation. Furthermore, with the microbeam X-ray diffraction, a practically single crystal-like diffraction pattern can be obtained, which permits the investigation of the detailed deformation process.[18-21]

In the polymer research, relation between molecular structure and macroscopic shape has practical importance. Although the deformational studies were reported by several authors [22-29], the relation is not yet systematically observed. From these points of view, we also studied contractive deformation of several polymers.

In this chapter, we shall separately present descriptions of cold-rolling deformation of the β-PP film [32] in the section 7.2, and contractive deformation of poly(ethylene terephthalate) (PET) [33] in the section 7.3.

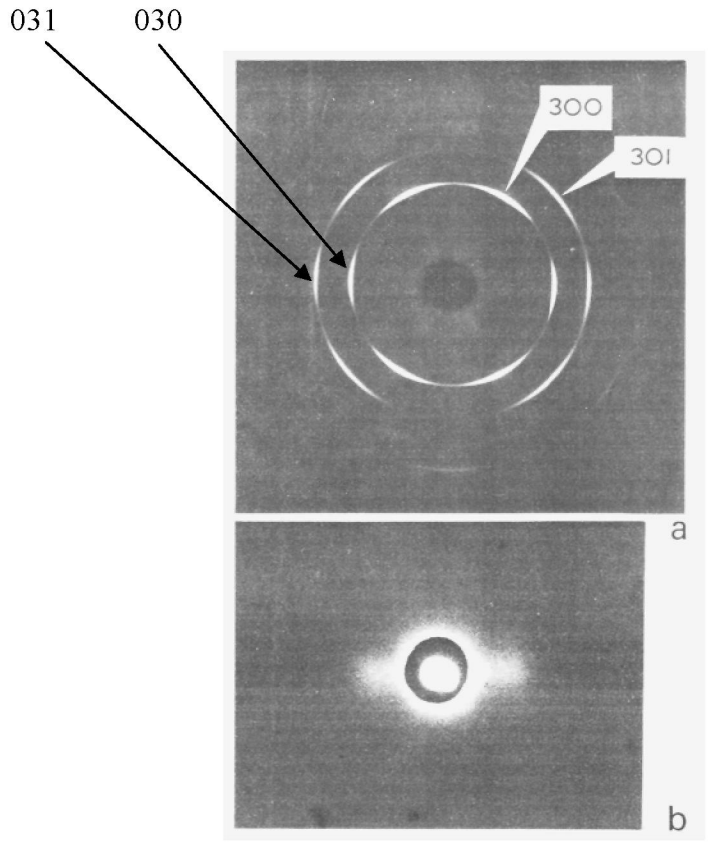

Fig. 7.1 (a) WAXS and (b) SAXS patterns from an oriented β-PP crystallized by the TSC method. Growth direction is vertical. Incident X-ray beam is perpendicular to the film surface [32]。

7.2 Cold-rolling of β-PP

7.2.1 Oriented β-PP crystallized by TSC

The β-phase material was produced by the TSC method [18,19] (See also chapter 5). Figures 7.1a and 7.1b represent the WAXS and SAXS patterns of the oriented β-PP, respectively. The growth direction is vertical. Indices in the WAXS pattern are based on the hexagonal lattice by Samuels *et al.* ($a = b$ =19.08 Å, c =6.49 Å) [17]. In Fig.7.1a, (300) and (030) reflections are on the inner ring and also (301) and (031) reflections outside. As a pair of (030) reflection exists on the equator, the oriented β-PP crystal has an a-axis orientation. It is known that the β-PP texture is composed of lamellar stacks. The SAXS pattern of Fig.7.1b shows that the lamellar normal is perpendicular to the growth direction. The long spacing measured by the SAXS is 230 Å in the ordinary sample with 250μm thickness, whereas it is 280 Å in the thick (800μm) sample.

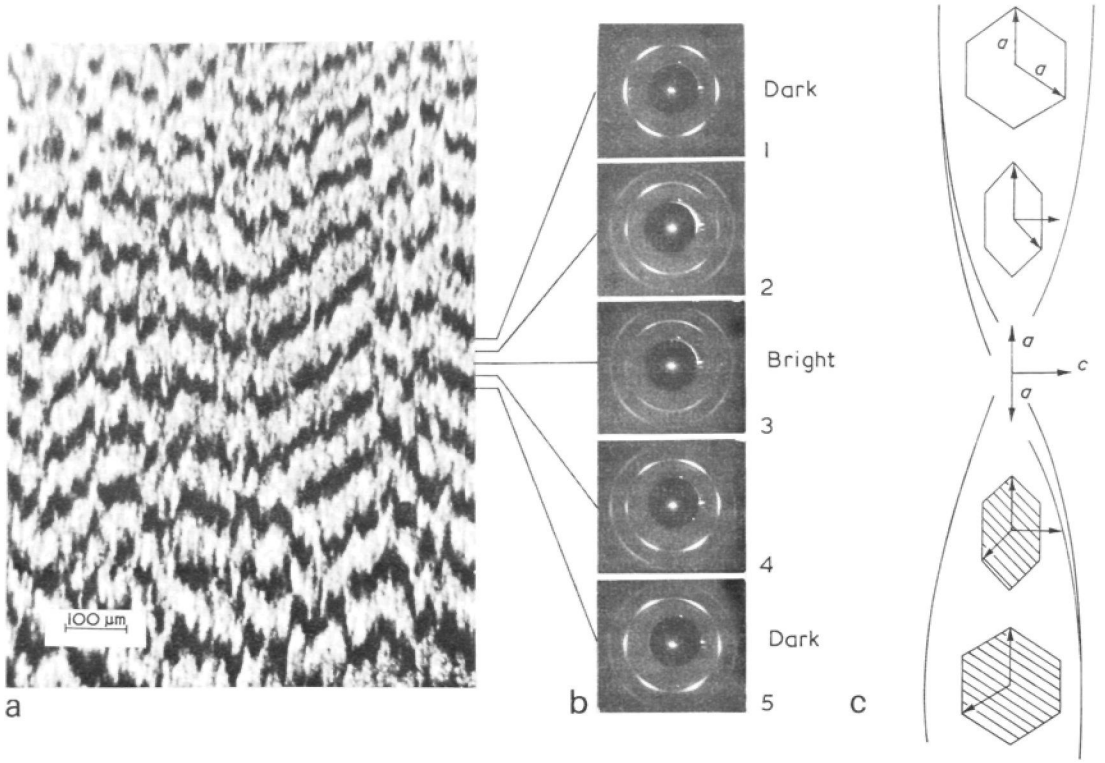

Fig. 7.2 (a) A polarization micrograph of an oriented β-PP sample, (b) micro-beam WAXS patterns along the growth direction at corresponding positions in the micrograph (Growth direction is vertical), and (c) rotation of β-PP lamellae with unit cells along the growth direction [32]。

A very thin sample with thickness of 10~20 μm was prepared by TSC for microscopic and microbeam X-ray diffraction observations. Polarization micrograph, as shown in Fig.7.2a, reveals the fibrils along the orientation direction with width of several 10 μm or less and contains bright and dark lateral stripes with a period of about 100 μm. A series of X-ray micro-diffraction experiments were carried out along the growth direction. The diameter of the incident X-ray is spotted in 15 μm. In Fig.7.2b are shown the micro-beam WAXS patterns with incident X-ray perpendicular to the film surface. The orientation of the β-PP crystal, analyzed from Fig.7.2b, is illustrated in Fig.7.2c. The results demonstrate that the *a*-axis is oriented parallel to the growth direction and that the *c*-axis (molecular axis) is perpendicular to it and is helically arranged along the *a*-axis. It is found that the c-axis is perpendicular to the sample film at the dark stripes and parallel at the bright stripes and that the period between the dark-dark and the bright-bright stripes corresponds to a 180° rotation of the *c*-axis. Therefore, in the β-PP film, the lamellae are helically rotated along the long axis with a pitch twice the period of stripes (~ 200 μm) as shown in Fig.7.2c. From the pattern of the stripe, the fibrils are cooperatively aligned in the same phase. These conditions are the same as those found in the case of PE spherulite [19,20].

7.2.2 Method of rolling and conditions of X-ray diffraction

For convenience of explanation of the rolling method, Cartesian coordinates are defined in the sample film as shown in Fig.7.3, namely X-axis perpendicular to the film surface, Y-axis parallel to the film surface and perpendicular to the lamellar axis (growth direction), and Z-axis parallel to the lamellar axis.

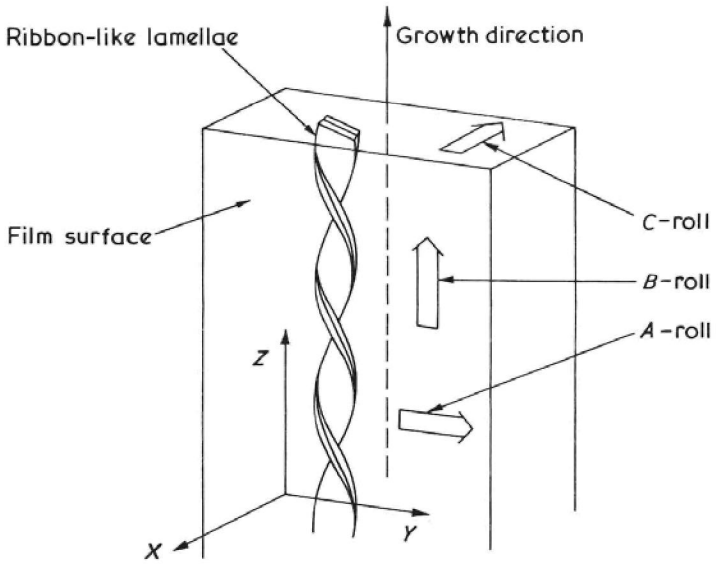

Fig.7.3 Definition of Cartesian coordinates relative to a sample plate and definition of the three rolling directions [32]。

Samples were rolled in three ways;

(i) A-roll: roll plane parallel to YZ plane and roll direction parallel to Y-axis,
(ii) B-roll: roll plane parallel to YZ plane and roll direction parallel to Z-axis,
(iii) C-roll: roll plane parallel to XY plane and roll direction parallel to X-axis.

The original thickness of the oriented β-PP film was 250 μm for the A- and B-roll deformation. In the case of C-roll measurement, we prepared a thick β-PP film (800 μm) by TSC. Strips of 250 μm in height were cut parallel to the XY plane from the thick film, and these strips were subjected to the C-roll deformation.

It is worthwhile to note that rolling changes the thickness and length of the sample. By measuring these quantities at each stage of rolling, thickness is found to vary inversely with the change in length. If we denote film thickness before and after the rolling as d_o and d, respectively, the draw-ratio (or roll-ratio) is defined by $\lambda = d_o/d$.

All the rolling processes were carried out at room temperature. The sample film was deformed by repeated rolling gradually narrowing gap of the rollers till the intended λ was finally attained. X-ray beam was passed through different directions of the sample rolled at different draw ratios. Based on the beam directions through the sample, we define WAXS and SAXS patterns. For instance, the X-ray patterns with the incident X-ray beam parallel to X-, Y-, and Z-axes are denoted to X-, Y-, and Z-patterns, respectively.

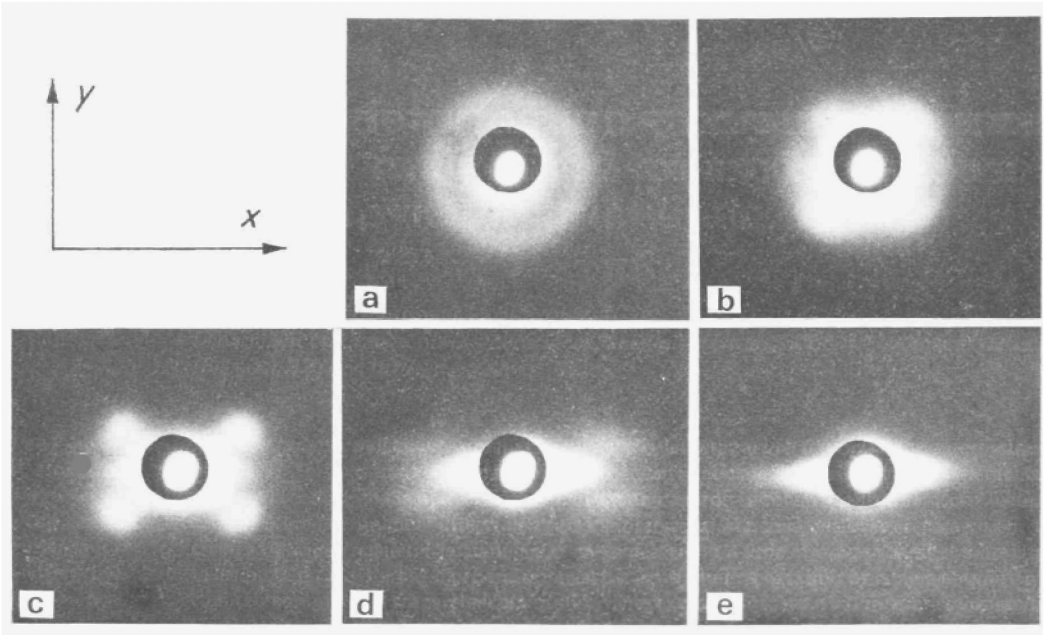

Fig. 7.4 SAXS Z-patterns of A-rolled samples at various draw ratios ; (a) λ = 1.0, (b) λ = 1.3, (c) λ = 1.9, (d) λ = 3.2, (e) λ = 5.3 [32]。

7.2.3 A-roll deformation

The X- and Y-patterns of SAXS measurements obtained from the original sample (λ = 1) are a typical two-point diagram as that observed in Fig.7.1b. In the X- and Y-patterns, the two-point diagram disappears at the initial stage of the deformation and no reflection maxima except the diffuse scattering around the incident beam are observed above λ =1.9. On the other hand, the Z-pattern of SAXS measurement at λ = 1 shows a uniform ring, which represents uniform distribution of lamellar normals around the Z-axis (Fig.7.4a). The Z-pattern varies with increasing λ, and the uniform ring splits into four separate parts which then change to a four-point diagram. In Fig.7.4b at λ = 1.3, a strong scattering is observed around the incident beam, and the intensity disappears on the meridian and decreases on the equator. The intensity increases at about 45° direction from the equator. The spacing (230 Å) obtained from the four-point maxima is still equal to the original one. At λ = 1.9, the four-point diagram becomes sharp and intense and is superimposed on an elliptical pattern.

The angle between Y axis and the intensity maximum of the diagonal spots is denoted to φ_A, which also represents the angle between Y-axis and the lamellar normal, as shown in Fig.7.5. Then, φ_A is measured to be 55 °, which is 10 ° larger than that at λ =1.3. The long spacing is reduced to 220 Å. Above λ = 1.9, the scattering around the incident beam shifts to the streak along the equator. At λ =3.2, the four-point lies on a fairly flat ellipsoid. The long spacing becomes about 160 Å. The values of the long spacing l and the angle φ_A at different λ are given in Table 7.1.

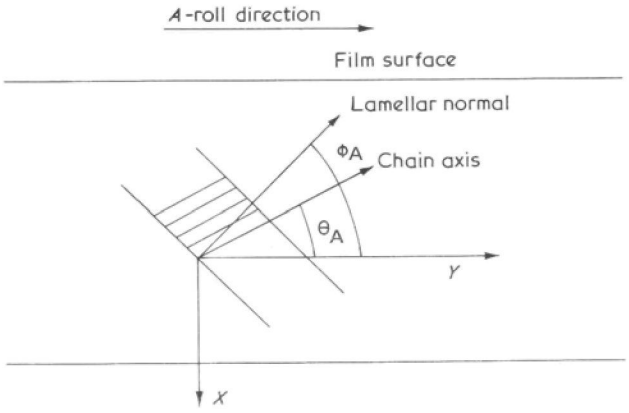

Fig. 7.5 Definition of φ_A and θ_A in the A-roll deformation [32].

Table 7.1 Values of long spacing, l, angles, φ_A and θ_A, in the A-roll [32]

Draw-ratio, λ	Long spacing, l (Å)	φ_A (°)	θ_A (°)	$\varphi_A-\theta_A$ (°)	cos ($\varphi_A-\theta_A$)	Ratio of long spacing, l/l_o
1.0	230	-	-	-	-	1.00
1.3	230	45	45	0	1.00	1.00
1.9	220	55	40	15	0.97	0.96
2.5	190	65	30	35	0.82	0.83
3.2	160	75	25	50	0.64	0.70
5.3	-	-	20	-	-	-

The orientation of the crystalline *c*-axis was observed by WAXS patterns. In the original sample, the crystalline *c*-axis is perpendicular to the lamellar surface, i.e., parallel to the lamellar normal. The corresponding WAXS Z-pattern of the original sample shows a uniform (030) ring, which indicates that the *c*-axis is rotated around the Z-axis corresponding to the helically twisting ribbon-like lamella. At λ =1.3, the (030) reflection almost disappears in the meridional and equatorial direction, while the intensity increases at the 45° direction. Here, the angle between the *c*-axis and the roll direction is denoted as θ_A as shown in Fig.7.5. In the initial stage of deformation, θ_A changes in good agreement with φ_A, which shows that the *c*-axis is rotated together with the rotation of the lamellae. With increasing λ, θ_A decreases and φ_A increases as shown in Table 7.1. Accordingly, the value of $\varphi_A - \theta_A$, which indicates the inclination of the crystalline *c*-axis with the lamellar normal, increases with λ. The values of $\varphi_A - \theta_A$ are also listed in Table 7.1.

The WAXS Z-pattern at λ = 3.2 is shown in Fig.7.6. The angle θ_A measured from the four distinct (030) reflections is ~ 25°. There are diffuse scatterings near the equator inside the (030) reflections, which seem to originate from imperfect α-phase microcrystallites reported by Peterlin *et al.* [11]. This reflection is denoted here to 'α-peak', which does not appear in the pattern of the original sample. The α-peak arises during the deformation and its intensity increases with increasing λ.

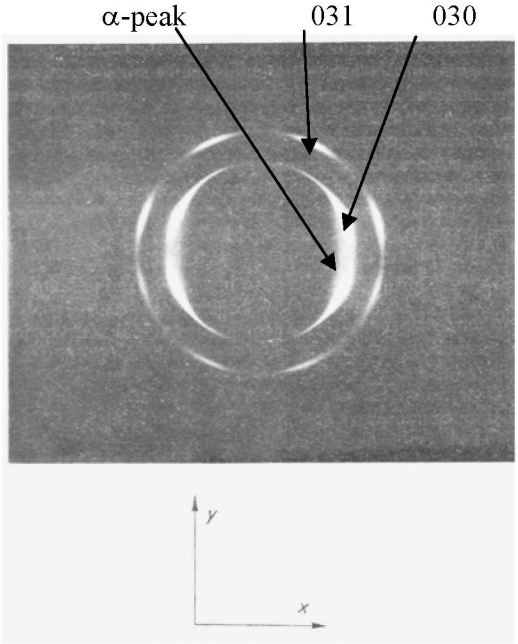

Fig. 7.6 WAXS Z-pattern of A-rolled sample at $\lambda = 3.2$; the roll direction (Y-axis) is vertical [32].

The highest draw-ratio λ, obtained in the range of uniform deformation, is about five. Beyond this value, microcracks arise in the sample, suggesting that further homogeneous deformation is not possible. The diffuseness and the streak in SAXS patterns beyond $\lambda = 5$ make it difficult to measure the long spacing. In the WAXS pattern at $\lambda = 5.3$, the β-phase reflections are still strong, while the α-peak increases its intensity.

In the SAXS and WAXS measurements of A-roll deformation, the Z-pattern was mainly observed. This pattern reveals the changes of both lamellar and chain orientations mostly in the XY plane. It seems that these changes are closely related to the macroscopic shape during the A-roll deformation, because the original sample was compressed along X-direction and elongated along Y-direction, without deforming along the Z-axis. It seems that plastic deformation of lamellar structure proceeds in parallel with that of the macroscopic shape.

The SAXS and WAXS patterns at $\lambda = 1.3$ strongly indicate that, at the first stage of the deformation, the lamellae are rotated in the XY plane without any reduction in their long spacing or any tilt of the *c*-axis. The fact that the intensity of SAXS spots at 45° direction increases at the early stage of deformation seems to indicate the existence of a quasistable state of lamellar orientation. When the lamellae are inclined to 45°, further rotation is prevented due to maximum shearing stress at 45°. The lamellar rotation by the inter-lamellar slip deformation has previously been reported in the spherulite deformation [7].

With increasing λ, the discrepancy between the angle φ_A and θ_A increases as shown in Table 7.1, which indicates that the *c*-axis is tilted within the lamellae. This fact suggests that both the interlamellar slip and the chain slip along the *c*-axis (inter-molecular slip) take place in the second stage of the deformation. When the *c*-axis is tilted within the lamellae, thickness of the crystalline lamellae decreases depending on cos $(\varphi_A - \theta_A)$. The values of cos $(\varphi_A - \theta_A)$ and of the ratio between long spacing and the original one, l/l_o, at each λ are also

compared in Table 7.1. They coincide with each other fairly well. The long spacing measured from the SAXS pattern represents the average period of the crystalline and amorphous layers. Normally, the change in the long spacing includes the change in thickness of the amorphous layer other than that of a crystalline layer. In spite of this fact, the good agreement between cos (φ_A–θ_A) and l/l_o indicates that the change in the long spacing is mainly due to tilt of crystalline *c*-axis within the lamellae.

An elliptical four-point diagram has been previously reported by other authors in slightly drawn linear polyethylene and other polymers [8-10]. This is due to the fact that the lamellae parallel to the roll plane are strongly reduced their spacing by compression.

The diffuse scattering around the incident beam seems to be a scattering from micro-voids formed by the deformation. These voids originate by breaking of lamellae, which is caused by movement of inter-lamellar or inter-molecular slip. In the case of slip between lamellae, particularly, the lamellae are partly broken by the tension of taut tie chains, and voids are formed in the vicinity when the stress is removed. The central streak, observed in the SAXS Z-pattern above λ = 1.9, indicates that the voids have no anisotropic shape. A central streak was also observed in the SAXS Y-pattern above λ =1.9, but certainly not in the X-pattern. Accordingly, the shape of the streak in the reciprocal space is long along the X-axis, which indicates that voids are expanded in the YZ plane.

In an observation of a thin film using a polarizing microscope, a remarkable change was recognized at the initial stage of the A-roll deformation. The bright and dark stripes seen in the original sample become indistinct and change to overall uniform brightness at λ = 1.5. This seems to coincide with the rotation of lamellae observed from SAXS and WAXS measurements, i.e. as a result of rotation, the crystalline *c*-axes at the bright and dark stripes are both inclined to about 45°. Thus the polarization micrograph changes to uniform appearance since all chains incline by the same angle.

The microbeam WAXS was carried out at positions of bright and dark stripes with a thin film A-rolled to λ = 1.5. The results also indicate that the chains, which are oriented originally parallel or perpendicular to the sample surface, are rotated about 45°. This agrees with the results obtained above.

From the above results, the deformation mechanisms of ***A-roll*** are summarized:

(1) In the first stage of deformation, ***rotation of lamellae*** occurs until almost all the lamellae are inclined about 45° to the roll direction. The deformation is proceeded by inter-lamellar slip as observed at λ = 1.3.

(2) In the second stage, the deformation is developed by both the ***inter-lamellar slip*** and inter-molecular slip along the *c*-axis as observed at λ = 1.9. As a result of the chain slip, the *c*-axis is tilted in the lamella and the long spacing decrease with increasing λ.

(3) The intensity of the α-peak increases with λ, showing that ***the β-phase crystals are partially broken*** and then imperfect α-phase is formed during the plastic deformation.

(4) The WAXS reflections from the β-phase crystals still exist even at λ =5.3.

7.2.4 B-roll deformation

The SAXS patterns at several stages of the B-rolled deformation are shown in Fig. 7.7. In the Z-patterns, the original uniform ring begins to disappear in the meridional direction at λ = 1.3. At λ = 1.9, the ring remains as arcs spreading over the range about ±45°

from the equator. At λ = 3.3, the reflection seems to lie on an ellipsoid. The long spacing measured from the remaining equatorial reflection does not change with λ.

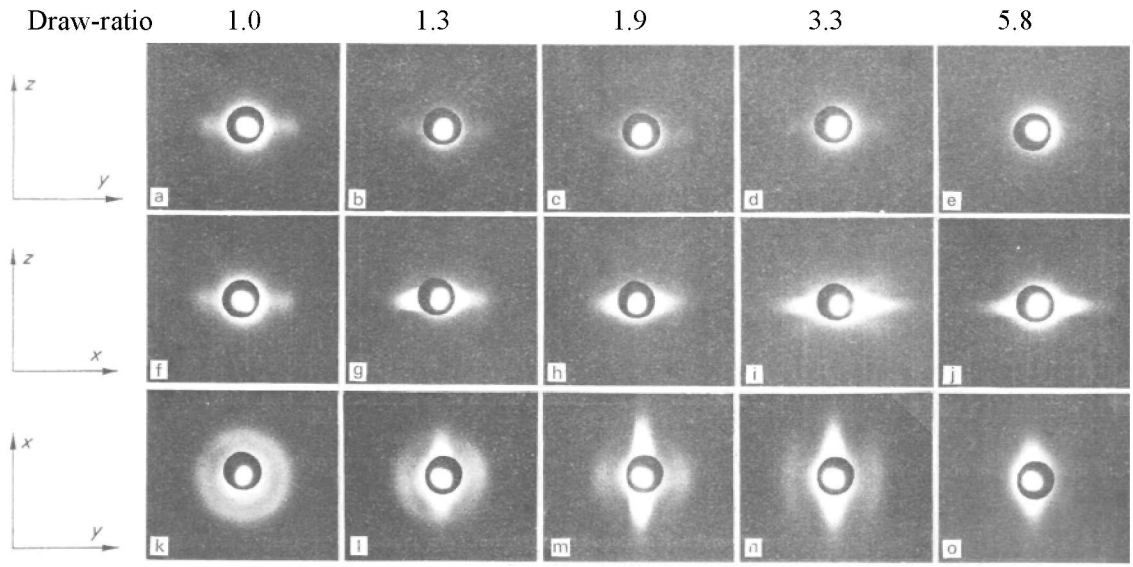

Fig. 7.7 SAXS X- (a)-(e), Y- [(f)-(j)], and Z- [(k)-(o)] patterns of B-rolled samples at various rolled-ratio, (a), (f), (k) λ = 1.0; (b), (g), (l) λ = 1.3; (c), (h), (m) λ = 1.9; (d), (i), (n) λ = 3.3; (e), (j), (o) λ = 5.8 [32].

On the other hand, in the SAXS Y-patterns gradually change to longitudinal arcs at λ =1.3 and thereafter to a very diffuse four-point diagram at λ =3.3. The observed maximum inclination of the lamellae is 20 ~ 30°. The original long spacing of 230 Å reduces to 200 Å at λ =3.3. In the X-patterns, the typical two-point diagram is preserved and the long spacing does not change until λ =3.3. At λ=5.8, the X-, Y-, and Z-patterns show no diffraction maxima. The central diffuse scattering or streak also appears in the SAXS Y- and Z-patterns above λ =1.3, where the streaks spread along the X-axis in the reciprocal space. This indicates that the shape of the micro-void is expanded in the YZ plane.

Here, we designate lamellae whose normal is parallel to the Y-axis in the original sample as E-lamella (edge-on-lamella) and the lamella whose normal is parallel to the X-axis as F-lamella (flat-lying lamella). E-lamellae and F-lamellae correspond to those at the central part of the bright- and dark-stripe in Fig.7.2a, respectively.

In the SAXS measurement, the reflection from the E-lamella appears mainly on the Y-patterns. The inclinations of all the lamellae are well shown in the Z-patterns. Considering that the crystalline *c*-axis is parallel to the lamellar normal in the original sample, it is known that the WAXS (300) and (030) reflections in the Y- and X-pattern are brought about chiefly from the E- and F-lamellae, respectively.

The results obtained from the SAXS X- and Y-patterns indicate that the E- and F-lamellae show different behavior during the B-roll deformation: the E-lamella remains unchanged both in the inclination and in the spacing, whereas the F-lamella inclines 30° in the XZ plane and the spacing decreases to 200 Å at λ = 3.3. The SAXS Z-pattern indicates that the deformation behavior of the intermediately positioned lamellae is a mixture of both types of deformation depending on their orientation.

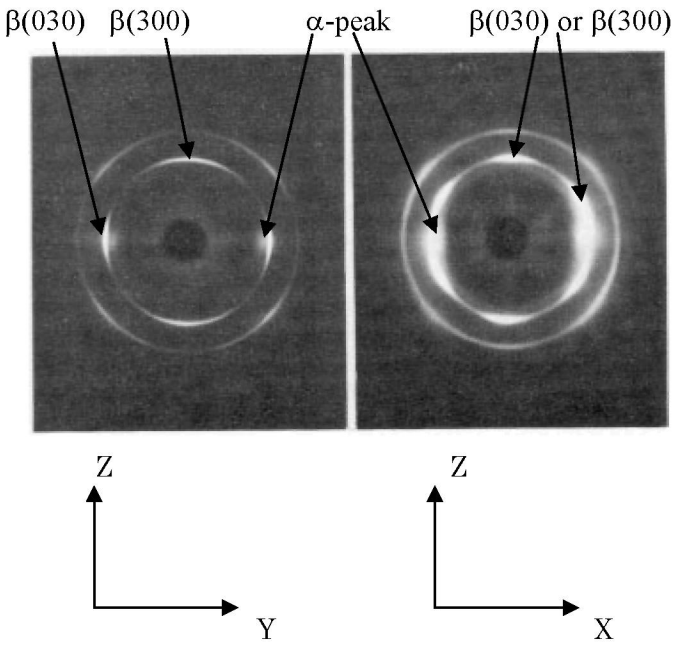

Fig. 7.8 WAXS (a) X-pattern and (b) Y-pattern of B-rolled sample at λ = 3.3; Z-axis is vertical. The inner ring is (300) or (030), the outer is (301) or (031). [32]

The WAXS X- and Y-patterns at λ =3.3 are shown in Fig.7.8. In the X-pattern, hexagonal symmetry (see Fig.7.1a) of the (300) and (030) reflections changes to four maxima; one pair are sharp equatorial arcs and another pair are broad and weak meridional arcs. The result indicates that the *c*-axis is tilted in the XZ plane. For measuring distribution of the c-axis, several WAXS patterns were taken varying the direction of the incident beam between X- and Z-axis. The inclination angle was thus determined 50 ~ 60° at λ = 3.3.

On the other hand, the Y pattern shows no evidence for the tilt of the *c*-axis except the rotation of (300) reflections around the Y-axis. This rotation ceases after exactly 30° rotation is attained and no further rotation occurs over λ = 3.3. The degree of orientation of the (300) reflection at λ = 3.3 is found to become sharper in comparison with that of the original sample (Fig.7.1a).

In the case of B-roll deformation, compression stress is imposed perpendicularly to the YZ plane and strain occurs mainly in the XZ plane. Accordingly, the chain axes of the E-lamellar crystals are perpendicular to the strain, so that the (300) $<1\bar{2}0>$ transverse slip is expected to be favored. The transverse slip perpendicular to the rod shaped molecules has been reported by Young [21] in the deformation of polytetrafluoroethylene hexagonal lattice. Because of the hexagonal symmetry of the crystalline form there are three possible (300) transverse slip systems at an angle of 60° to each other. The slip will take place in the (300) plane which experiences the highest shear stress. As a result of the transverse slip, the crystal rotates until this plane is inclined by 60° to the compression direction. At this angle, another (300) plane is also inclined at 60° to the X-axis and slip then takes place on both of these planes alternatively. This type of deformation is known as the duplex slip. After the rotation by 60°, the (300) peak is concentrated by restriction of further rotation.

In the WAXS X- and Y-patterns at $\lambda = 3.3$ (Fig.7.8), diffuse reflections are observed inside the β-phase (300) reflections, which are the α-peaks as observed in the A-roll deformation. The α-peak appears during the deformation on the equator of WAXS X- and Y-patterns and its intensity increase with increasing λ. It is considered, like in A-roll, to originate from imperfect α-phase whose *c*-axis is oriented parallel to Z-axis.

Observations by the polarizing microscope were carried out for the B-rolled thin film. The spacing of the dark and bright stripes is found to extend by the deformation, but, unlike A-roll, the stripes are visible even at $\lambda = 5.0$. This may be related to the different deformation mechanisms in the dark (F-lamellae) and bright (E-lamellae) stripes. The microbeam WAXS measurement indicated that the orientation of the β-phase molecule is different in the dark and bright stripes, which is consistent with the results obtained by the above experiments.

The results of the ***B-roll*** deformation are summarized as follows:

(1) ***B-roll deformation is different in the E- and F-lamellae.***

(2) In the F- and the neighboring lamellae (dark stripe), the deformation develops mainly by ***the chain slip along the chain direction***, resulting in the tilting of c-axis together with the lamellar inclination.

(3) In the E- and the neighboring lamellae (bright stripe), the deformation develops by the (300) $<1\bar{2}0>$ transverse slip without any inclination of the *c*-axis and the lamellar normal. As the consequence of the ***duplex slip***, the degree of orientation of (300) reflections is increased during the deformation.

(4) In the intermediate lamellae oriented between the E- and F-directions, the above mechanisms may operate simultaneously depending on their orientation.

(5) During the B-roll deformation, the α-peak increases with λ.

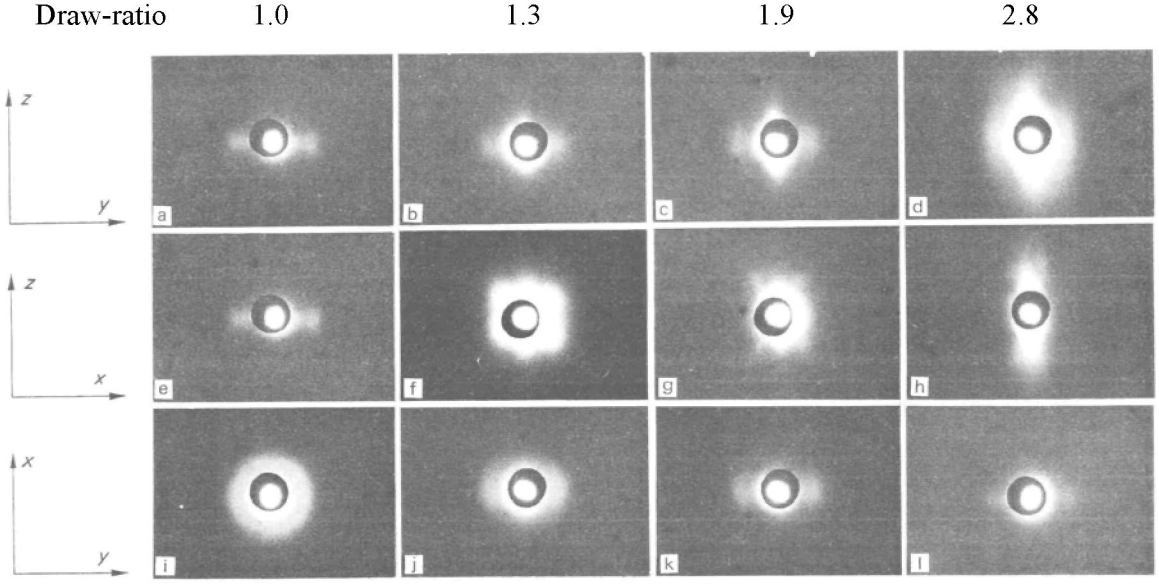

Fig. 7.9 SAXS X- [(a)-(d)], Y- [(e)-(h)], and Z- [(i)-(l)] patterns of C-rolled samples at various rolled-ratios, (a), (e), (i) $\lambda = 1.0$; (b), (f), (j) $\lambda = 1.3$; (c), (g), (k) $\lambda = 1.9$; (d), (h), (l) $\lambda = 2.8$ [32].

7.2.5 C-roll deformation

In Fig.7.9, the SAXS patterns are shown at several stages of λ during C-roll deformation. In the Z-patterns, the uniform ring at $\lambda = 1$ changes to equatorial arcs at $\lambda = 1.3$ and to a two-point diagram at $\lambda = 1.9$ and 2.8, which indicates that the lamellae normals are inclined from the XY plane except the E-lamellae. There was no change in the spacing of the E-lamllae even at $\lambda = 2.8$. On the other hand, in the Y-patterns, the lamellae normal is largely inclined with λ. The two-point pattern of the original sample changes to the four-point pattern at $\lambda = 1.3$. Both the angle (φ_C) of the lamellae normal with respect to the X-axis and the long spacing (l) measured from the Y-pattern change with increasing λ as shown in Table 7.2. The two-point diagram in the X-patterns does not change with $\lambda = 1.9$ but then the points extend to arcs along the meridianal direction at $\lambda = 2.8$. The streak along the Z-axis are observed in the X- and Y-patterns above $\lambda = 1.3$, showing that the micro-voids are expanded in the XY plane.

Table 7.2 Values of long spacing, l, angles, φ_C and θ_C, in the C-roll [32]

Draw-ratio, λ	Long spacing, l (Å)	φ_C (°)	θ_C (°)	$\varphi_C - \theta_C$ (°)	$\cos(\varphi_C - \theta_C)$	Ratio of long spacing, l/l_o
1.0	280	0	0	0	1.00	1.00
1.3	250	35	~10	~25	~0.97	0.89
1.9	240	50	~20	~30	~0.87	0.86
2.8	220	75	~40	~35	~0.82	0.79

The WAXS Y-pattern at $\lambda = 2.8$ shows that the position of the hexagonally situated (300) reflections is unchanged before and after the deformation, but the degree of orientation increases with deformation. This fact indicates that the crystals in the E-lamellae are deformed by the (300) $<1\bar{2}0>$ transverse slip in the same manner as observed in the B-roll deformation, and that the alignment of the (300) plane is improved by the duplex slip. In this case, however, the original orientation of three (300) slip planes, which are parallel and 60° to the compression direction, is just suitable for the duplex slip. Accordingly, the Y-pattern after deformation does not show any rotation of the (300) reflections.

The WAXS X-pattern at $\lambda = 2.8$ shows that the c-axis is rotated in the XZ plane. It is difficult to measure the precise inclination angle for the same reason as noted in the WAXS X-pattern of the B-rolled sample. This angle (θ_C) is estimated by the same procedure as that in the B-roll deformation and included in Table 7.2.

The results of SAXS and WAXS measurements suggest that the normal of the F-lamellae is easily rotated in the XZ plane at the early stage of the deformation, whereas the c-axis is largely tilted in the F-lamella and the long spacing is reduced by this tilt in the same manner as that interpreted in the A-roll deformation. In the X- and Y-patterns at $\lambda = 2.8$, the α-peaks also appear on the equator inside the (300) reflection but their intensity is weaker than that observed in the A- and B-roll deformation.

We have following summaries of the ***C-roll*** deformation:

(1) In the early stage, almost all the lamellae except the ***E-lamellae are inclined by the chain slip along the c-axis***. The lamellar normals are rotated in the XZ plane, and the long spacing decreases by the chain tilt with increasing λ.

(2) On the other hand, in the ***E-lamellae***, deformation develops by the (300) $<1\bar{2}0>$ transverse slip, and neither the lamellae normal nor the *c*-axis are inclined during the ***duplex slip***.

(3) By the plastic deformation of β-PP, α-peak increases with λ.

7.2.6 Anisotropic character of lamellar deformation

In the bulk polymer, spherulitic structure is occupied in the sample. If we consider the rolling of the bulk sample, the spherulite is subjected to deform. As illustrated in Fig.7.10, ribbon-like lamellae are developed from the center of the spherulite. Then the A-, B- and C-roll deformations are simultaneously observed by the lamellae oriented along y-, z- and x-direction, respectively. The anisotropic behavior of plastic deformation appears depending on the lamellar orientation.

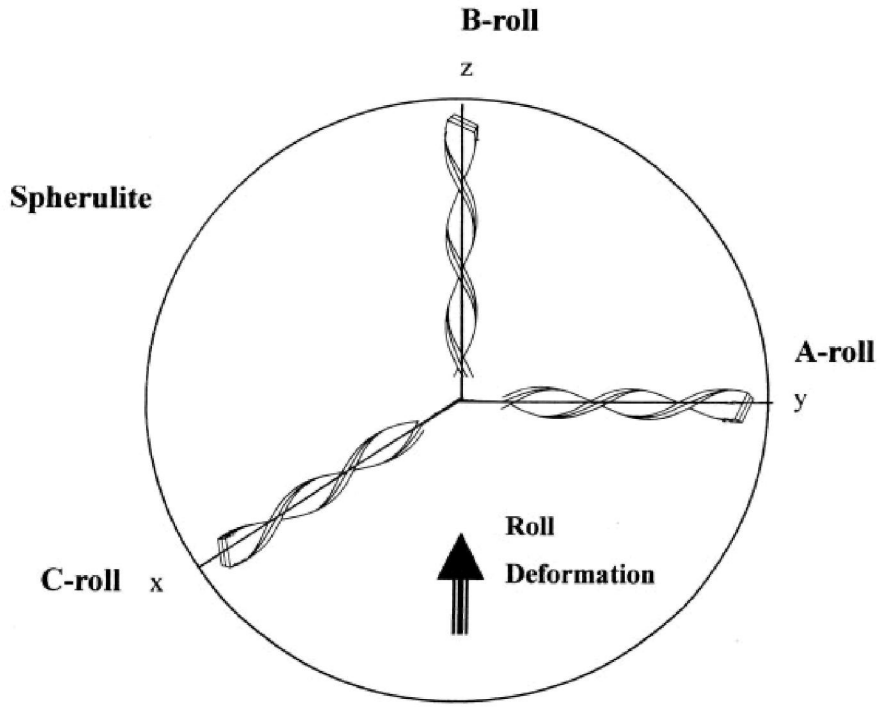

Fig. 7.10 Ribbon-like lamellae developed in the spherulite.

In the present research using the oriented lamellae prepared by TSC, both E- and F-lamellae are rotated by 45° at λ =1.3 and successive inter-lamellar and inter-molecular slip deformation at λ=1.9 are observed in A-roll. The E-lamellae are deformed by the transversal duplex slip above λ=1.9 in B-roll. In the C-roll, F-lamellae are easy to incline at λ=1.3, whereas the E-lamellae are subjected by the duplex slip in the same manner as B-roll.

From these results, the probable plastic deformation in the spherulitic sample is possible to develop in the F-lamellae of C-roll (fibrils parallel to x-direction), then lamellar rotation in A-roll (fibrils parallel to y-direction), followed by the inter-molecular slip in A-roll and transversal duplex slip in B- and C-roll (fibrils parallel to z- and x-directions).

7.2.7 Effect of annealing after deformation

The samples stretched by the rolling deformation were annealed under tension for 2h at 120 °C, which is about 30 °C lower than the melting temperature of the β-PP crystal. The WAXS X-patterns of the B-rolled sample before and after the annealing are shown in Fig.7.11. Both the intensity and the sharpness of the reflections from the β-phase crystal do not show any change. However, those of the α-peak strongly increase by the annealing, which indicates that the perfection of the α-phase crystallites is enhanced by the annealing. These results show that the α-phase crystallites are organized by unfolding or partial melting of the β-phase lamellae in the process of the roll deformation.

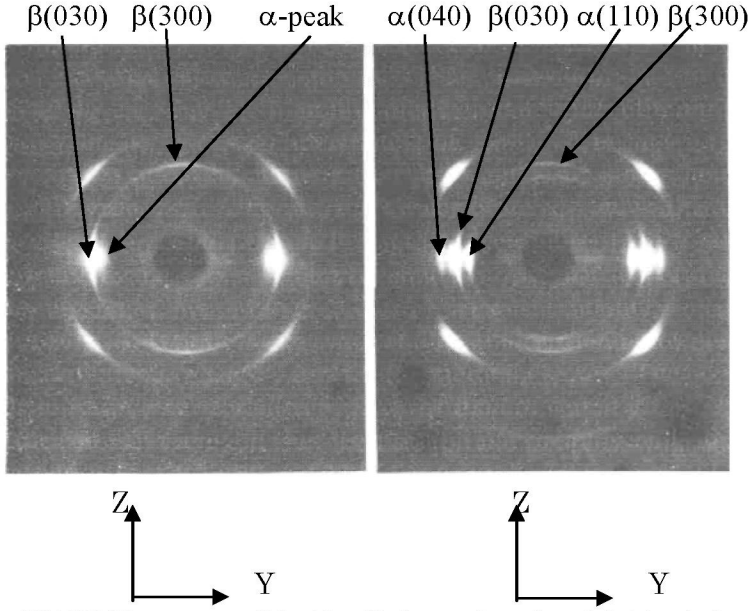

Fig. 7.11 WAXS X-patterns of the B-rolled sample at λ = 5.8; Z-axis is vertical, (a) before and (b) after annealing treatment at 120 °C. [32]

7.2.8 Transformation from a- to c-axis orientation

Generally speaking, when bulk material is stretched by drawing or rolling, the molecules in the crystallite are aligned to the stretching direction and finally attained to the *c*-axis oriented structure. In our case, the starting material is *a*-axis-oriented β-PP. Here, we discuss the mechanism of transformation from *a*- to *c*-axis orientation. The problem to be solved is whether blocks of the original lamellar structure are directly incorporated into the new lamellar structure, or whether the molecules recrystallize after unfolding or melting of the original structure.

Peterlin *et al.* [10] observed meridional reflections of SAXS for specimens of λ = 5 in the case of rolling deformation of polyethylene, which originate from a new lamellar structure composed of *c*-axis-oriented molecules. For the rolling deformation of β-PP in our case, however, the β -phase did not show perfect *c*-axis orientation even for λ > 5. Besides,

from the SAXS patterns, it is shown that the lamellar normal tends to lie perpendicular to the rolling direction with increasing λ instead of orienting to the rolling direction. During the roll deformation, no meridional reflection corresponding to the new lamellar structure by Peterlin *et al.* is observed even for a large λ. After an additional heavy roll deformation (A- and B-roll) such as λ = 7 ~ 10, no SAXS reflection was found on the meridian.

The results of β-PP strongly indicate that there is no c-axis oriented β-PP after the roll deformation. Accordingly, the deformed structure in our case seems to be quite different from the newly built lamellar structure generally seen in polyethylene or in other polymers. On the other hand, the α-phase crystallites, yielded by local unfolding or melting of molecules of β-phase lamellae as seen from WAXS patterns, show perfect *c*-axis orientation.

Accordingly, the deformation in β-PP must be followed by the phase transformation from β- to α-crystal. As already referred in the 'Introduction' (section 7.1), this β→α transformation implies that the β-phase must once be destroyed by unfolding or melting, owing to the difference of molecular conformation between these two crystals.

With the above considerations, it is concluded that, in the case of roll deformation of β-PP at room temperature, ***the transformation from a- to c-axis orientation takes place not through breaking up of the original lamellae into blocks and incorporating into the new lamellae, but through unfolding or melting of the original texture and subsequent re-crystallization.***

7.3 Contractive Deformation of Drawn PET

7.3.1 Experimental setup

Figure 7.12 shows a schematic diagram of the experimental apparatus for measuring the contractive deformation. Two weights W_1 and W_2 were counterbalances, used to measure the contractive deformation under unloading condition. The sample was fixed with W_2 and a clamp. The thermally controlled silicon oil bath was mechanically lifted up at the rate of 30 cm/sec. When the silicon oil bath was lifted, the sample was immersed in it within 0.1 sec.

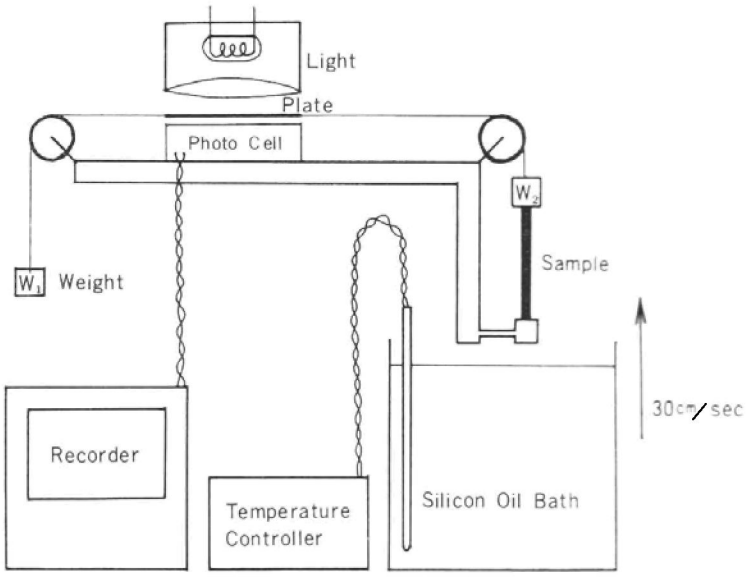

Fig. 7.12 A scheme for measuring contractive deformation [33].

By the heating, macroscopic shape of the sample was changed, which accompanied the movement of the plate. As a photo-cell is covered by the plate, the movement was measured by the recorder. Preliminary measurements showed that inertia of the weights and friction of the apparatus influenced negligibly to the contractive deformation.

7.3.2 Sample drawing

The quenched PET shows an isotropic and amorphous state at room temperature. The amorphous film is transparent and hard at room temperature, whereas it becomes soft above its glass transition temperature (69 °C).

The amorphous PET film was drawn by the following two ways:

i) Cold-drawing at room temperature through the necking stage, with the drawing speed and the draw ratio of 0.1 mm/sec and 4.0, respectively.

ii) Hot-drawing at 80 °C in a thermally controlled water bath with the drawing speed and the draw-ratio of about 1.0 cm/sec and 4.0, respectively.

By annealing the sample, the drawn PET was enhanced the crystallinity. The drawn samples were then annealed in a taut state (without shrinkage) at the annealing temperature T_A for 1 h. The contractive deformation was measured at heating temperature T_H which was usually higher than T_A. The length of the oriented sample is 15–20 mm before the contraction.

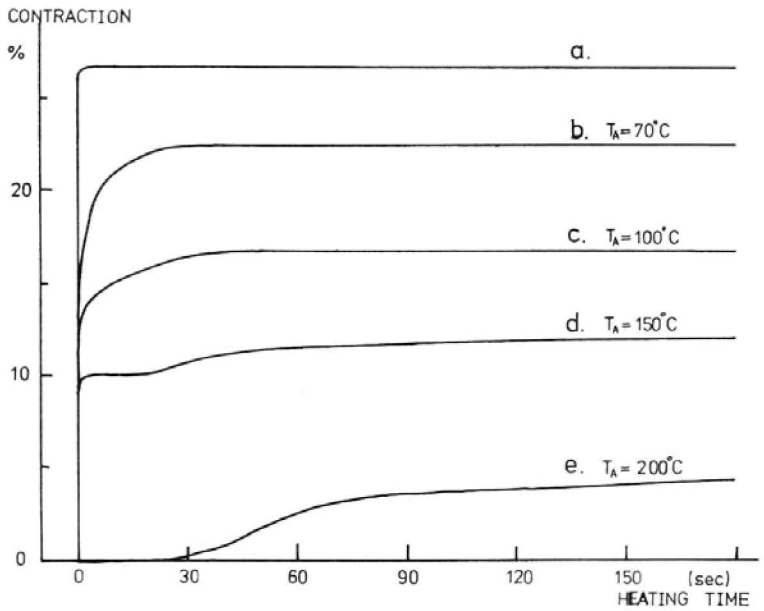

Fig. 7.13 Contraction curves at T_H = 235 °C for the drawn PET sample, (a) without annealing and annealed at (b) 70 °C, (c) 100 °C, (d) 150 °C and (e) 200 °C. [33]

7.3.3 Contraction of the cold drawn PET

The contractive behaviors of PET samples, drawn at room temperature and annealed at various temperatures, were measured at the heating temperature of 235 °C. The observed contraction, which is normalized by the length of the sample before heating, is shown in Fig.7.13 as a function of heating time. The contraction (%) is seen to vary depending on T_A.

The final value of contraction, which is less than 30%, decreases with increasing T_A.

In case of the sample without annealing, rapid contraction occurs within 5 sec after which no contraction is observed (Fig.7.13a). In case of the annealed samples at 70 °C and 100 °C, contraction curves are slowly approached to the maximum value (Figs.7.13b and c) On the sample annealed at 150 °C, secondary slow contraction appears after quick contraction (Fig.7.13d). The quick contraction disappears and only the slow one is observed when the sample is annealed at 200 °C (Fig.7.13e): As the quick contraction decreases with T_A, it depends on the amount of amorphous molecules.

7.3.4 Contraction of the hot drawn PET

Contractive behaviors of the PET samples drawn at 80 °C were measured at T_H =100 °C . In Fig.7.14a, negative contraction (elongation) appears after the quick contraction. In the case of T_H =200 °C, with a low quick contraction, the final length is extended in Fig.7.14b. Considering the effect of the counter-balance, the hot-drawn PET is deformed by a special (self-elongation) mechanism.

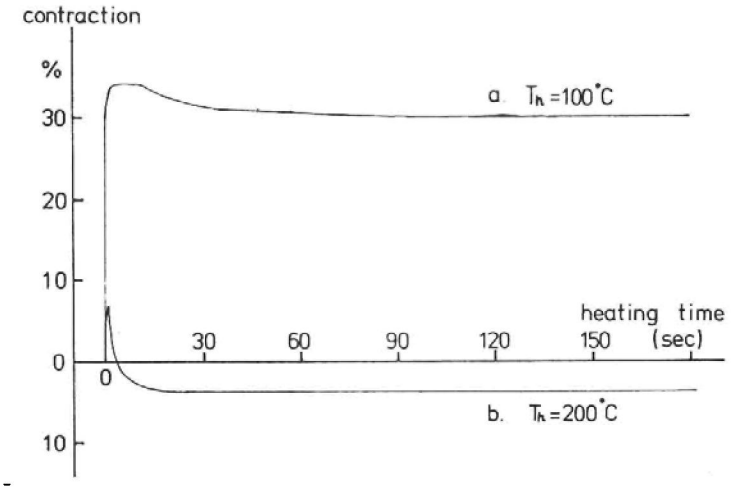

Fig. 7.14 Contraction curve of PET drawn at 80 °C; T_H is (a) 100 °C and (b) 200 °C. [33]

7.3.5 X-ray diffraction measurements during the contraction

WAXS and SAXS measurements of the samples were carried out during the contraction. For the cold-drawn sample annealed at 150 °C, X-ray patterns are obtained in the process of the contractive deformation at 235 °C. Then, the contraction is stopped at the stage shown by arrows in Fig.7.15. The results show that the crystalline orientation is rarely changed after the quick contraction (Fig. 7.15c) and the secondary slow contraction (Fig. 7.15e). The typical 4-point SAXS patterns show that the inclined layer structure develops during the quick and slow contraction. The long spacing obtained from the SAXS patterns changes from 105Å (Fig.7.15b) to 119Å (Fig. 7.15d) and 124Å (Fig.7.15f). During the contraction, the inclined layer and crystalline orientation are preserved. Then, the mechanism of quick contraction is due to relaxing of amorphous molecules, which enhances to develop layers during the slow contraction.

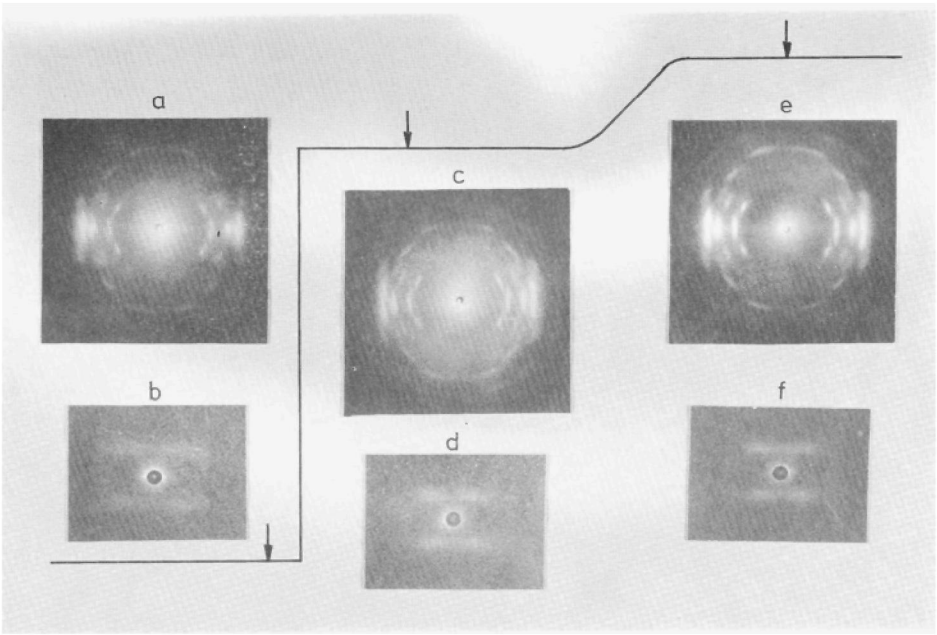

Fig. 7.15 WAXS and SAXS patterns of the cold-drawn PET annealed at 150 °C. The contraction was performed at 235 °C and X-ray measurements were done at the arrowed positions: a),b): before contraction, c),d):after the quick shrinkage, and e), f): after the slow shrinkage. [33]

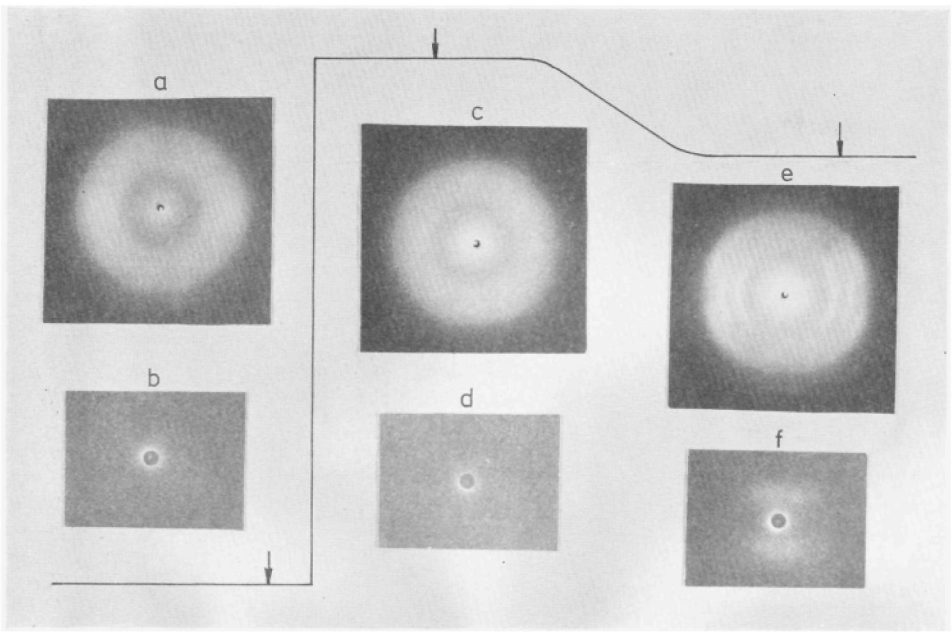

Fig. 7.16 WAXS and SAXS patterns of the hot-drawn PET at 80 °C. The contraction was performed at 150 °C and X-ray measurements were done at the arrowed positions: a),b): before contraction, c),d):after the quick shrinkage, and e), f): after the slow elongation. [33]

WAXS patterns of hot-drawn PET at 80 °C indicate that, during the quick contraction, the amorphous orientation disappears (Fig.7.16c). Then reorientation and crystallization arise after the negative contraction (Fig.7.16e). The diffuse crystalline arcs in Fig.7.16e indicate that the crystalline molecules are highly inclined in the layer. During the quick contraction, SAXS pattern has no intense peak (Fig.7.16d). The 2-point SAXS pattern (Fig.7.16f) indicates that the flat layer is formed by the negative contraction. From the results, flat layer with inclined molecules enhances the self-elongation in the macroscopic shape.

In order to compare the original orientation, WAXS patterns are measured in the as-drawn samples. The cold-drawn sample (Fig.1.17a) has a strong intensity peaks on the equator showing that molecules are highly oriented along the draw-direction. On the other hand, the hot-drawn sample shows nearly isotropic diffuse ring. For measuring the intensity distribution, reflection angles 20±2° was integrated as a function of the azimuthal angle (Fig.7.17b). The intensity distribution of Fig.7.18 has a sharp peak in the cold-drawn PET, whereas broad one in the hot-drawn sample.

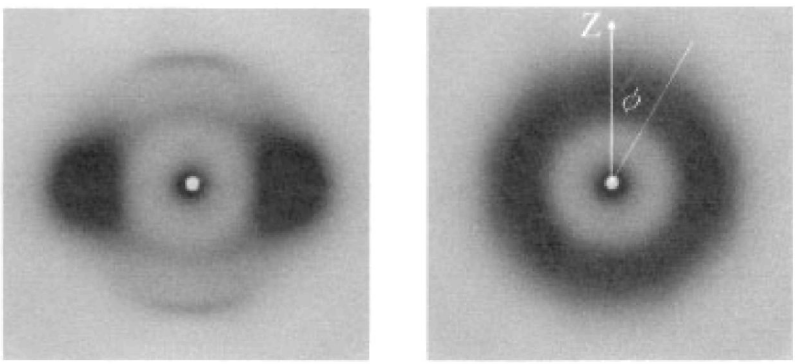

(a) Cold drawn PET (b) Hot drawn PET

Fig. 7.17 WAXS patterns of the as-drawn PET

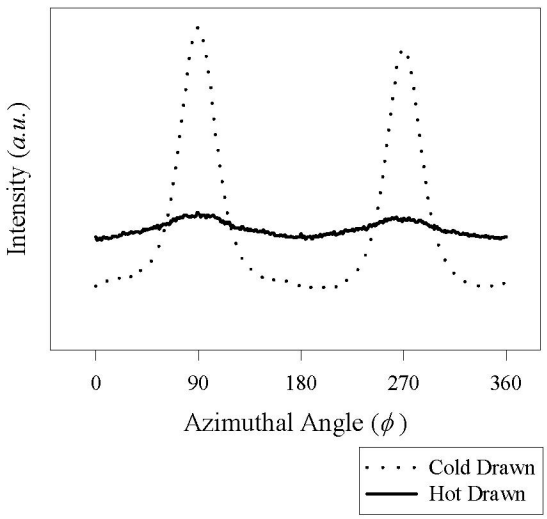

Fig.7.18 Intensity distribution of the as-drawn PET

7.3.6 Relation between contractive deformation and internal structure

From the above measurements on PET at different annealing and heating conditions, the contraction is distinguished into two patterns:

(i) The quick contraction appears at the initial stage of the deformation: The quick contraction is defined here A-type.

(ii) The secondary and slow deformation is followed, which is further separated to the positive and negative contraction: The slow contraction or elongation is defined B-type.

(iii) Normally, the contraction patterns show mixture of the above two types: C-type.

In an oriented material, like rubber, the free energy becomes higher due to the low conformational entropy of the oriented molecules. Consequently, A-type is caused by the rubber-like contraction of the oriented amorphous molecules. In the case of polymers, the rubber-like contraction is restricted by development of the crystalline substances, which is shown by the fact that the final value of the contraction is less than 30% and that the contraction decreases with annealing treatment. In annealed samples, however, A-type still occurs as far as the oriented amorphous substance remains in it.

The experimental results suggest that B-type is closely related to the development of the crystalline layer structure. The possible model of the B-type deformation, which is based on the results of X-ray diffraction measurements, is proposed in Fig.7.19.

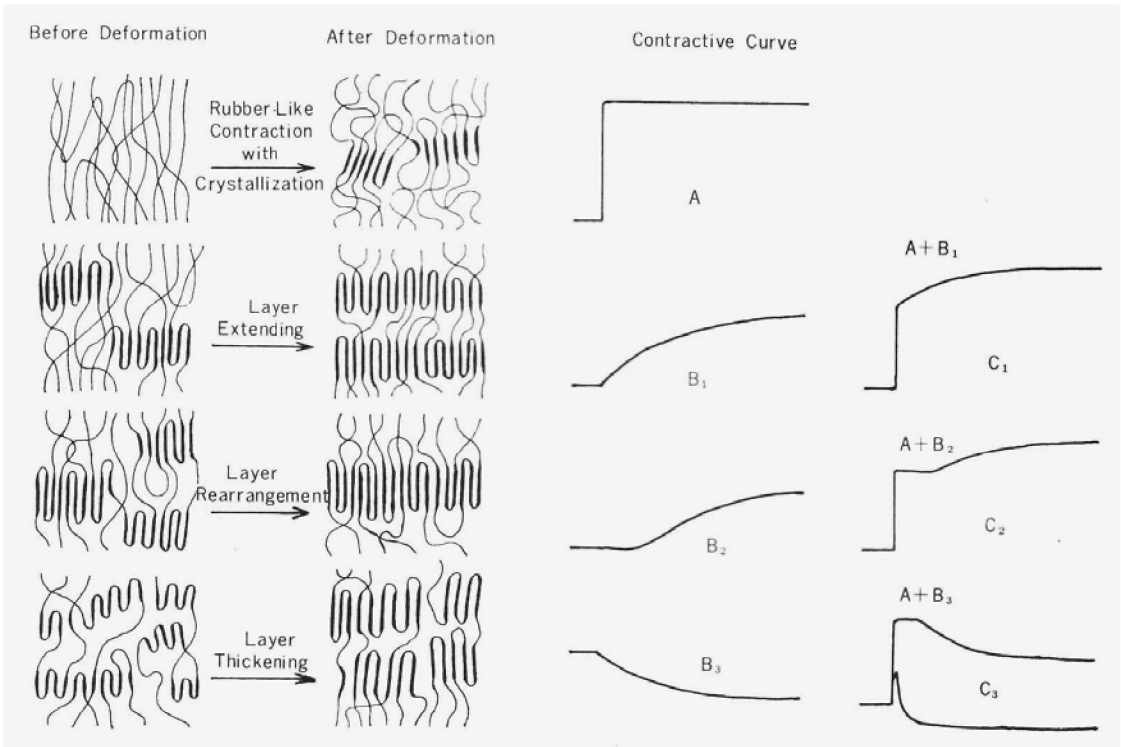

Fig. 7.19 Possible models of the contractive deformations. Bold lines represent the crystalline molecules [33]

In Fig.7.19, the contractive curves are further classified into several types :

1. ***A-type***: The quick contraction observed in the initial stage of the deformation, which is decreased with T_A. A-type seems to occur by the rapid transformation of oriented amorphous conformation into unoriented one. This type is the same mechanism as known by the rubber elasticity [30,31]. During A-type, amorphous molecules are relaxed in orientation. In the cold-drawn PET, A-type is accompanied by the oriented crystallization at high T_H.
2. ***B_1-type***: The slow contraction appeared continuously after A-type. B_1-type appears in the cold-drawn sample, which is caused by oriented crystallization into an inclined layer structure with highly oriented molecules (represented by the 4-point structure; see chapter 4). During the layer formation, disordered conformation, such as entanglement and folding, is removed by the regular crystal and concentrated in the amorphous layer. By heating at T_H, secondary contraction occurs by further relaxation of oriented amorphous conformation.
3. ***B_2-type***: The slow contraction appeared after a lag time in the cold-drawn sample. The difference between B_1- and B_2-type is the appearance of the time lag; suggesting that B_2-type is required by rearrangement (recrystallization) of the layer structure by melting thin layers. During the rearrangement, macroscopic contraction appears by the same reason of B_1-type.
4. ***B_3-type***: The slow elongation appeared in the hot-drawn sample. Flat layers with inclined molecules (represented by the 2-point structure; see chapter 4) are developed during B_3-type. Original degree of orientation is low in the hot-drawn sample. Consequently, secondary contraction, such as B_1- and B_2-type, is not required during the layer formation. On the contrary, the flat layers will be foundation of the macroscopic structure, which enhances self-elongation.
5. ***C_1-type***: Mixture of A- and B_1-type. (Rubber-like contraction + Inclined layer formation)
6. ***C_2-type***: Mixture of A- and B_2-type. (Rubber-like contraction + Rearrangement of layers)
7. ***C_3-type***: Mixture of A- and B_3-type. (Rubber-like contraction + Flat layer formation)

Macroscopic contraction may arise when material flow occurs from the length to the width, and macroscopic elongation may take place when material flow occurs in the opposite direction. In the cold drawn sample, highly oriented amorphous shows the leading role of the contraction. In the secondary step, relaxation of amorphous layer is brought about contraction observed in B_1- and B_2-type. On the other hand in B_3-type, material flows in the direction of extension by the formation of flat layers.

References

1. I. L. Hay and A. Keller, *Kolloid Z. Z. Polym.*, **205**, 43 (1965)
2. P. H. Geil, *`Polymer Single Crystals`*, Interscience, New York, p 445 (1964)
3. H. Kiho, A. Peterlin, and P. H. Geil, *J. Appl. Phys.*, **35**, 1599 (1964)
4. A. Peterlin, P. Ingram, and H. Kiho, *Makromol. Chem.*, **86**, 294 (1965)
5. K. Kobayashi, and T. Nagasawa, *J. Polym. Sci.* (*C*), **15**, 163 (1966)
6. R. Corneliussen, and A. Peterlin, *Makromol. Chem.*, **105**, 193 (1967)
7. A. Peterlin, *Kolloid Z. Z. Polym.*, **233**, 857 (1969)
8. A. Peterlin, and F. J. Baltá-Calleja, *J. Appl. Phys.*, **40**, 4238 (1969)

9. G. Meinel, N. Morosoff, and A. Peterlin, *Kolloid Z. Z. Polym., (A-2)*, **8**, 1723 (1970)
10. G. Meinel and A. Peterlin, *Kolloid Z. Z. Polym.*, **242**, 1151 (1970)
11. N. Morosoff and A. Peterlin, *J. Polym. Sci. (A-2),* **10**, 1237 (1972)
12. K. Sakaoku, N. Morosoff and A. Peterlin, *J. Polym. Sci. (Polym. Phys. Edn),* **11**, 31 (1973)
13. A. Peterlin, Kolloid Z. *Z. Polym.*, **253**, 809 (1975)
14. R. J. Young, P. B. Bowden, J. M. Ritchie, and J. G. Rider, *J. Mater. Sci.*, **8**, 23 (1973)
15. D. P. Pope and A. Keller, *J. Mater. Sci.*, **9**. 920 (1974)
16. A. Turner-Jones, Z. M. Aizlewood, and D. R. Beckett, *Makromol. Chem.*, **75**, 134 (1964)
17. R. J. Samuels and R. Y. Yee, *J. Polym. Sci (A-2),* **10**, 385 (1972)
18. K. Tanaka, T. Seto, and Y. Fujiwara, *Rep. Prog. Polym. Phys. Jpn.*, p 285 (1963)
19. Y. Fujiwara, *Kolloid Z. Z. Polym.,* **226**, 135 (1968)
20. Y. Fujiwara, *J. Appl. Polym. Sci.*, **4**, 10 (1960)
21. R. Young, *J. Polymer*, **16**, 450 (1975)
22. P. H. Geil, *J. Polym. Sci.*, **A2**, 3813 (1964)
23. I. L. Hay and A. Keller, *Kolloid-Z, Z. Polym.*, **204**, 43 (1965)
24. K. Sakaoku and A. Petrlin, *J. Macromol. Sci. Phys.*, **1**, 103 (1965)
25. F. J. Baltá Calleja and A. Peterlin, *J. Appl. Phys.*, **40**, 4238 (1969)
26. K. O'Leary and P. H. Geil, *J. Macromol. Sci. Phys.*, **B2**, 261 (1968).
27. W. O. Statton, J. L. Koenig and M. Hannon, *J. Appl. Phys.,* **41**, 4290 91970)
28. K. H. Illers, *Macromol. Chem.*, **118**, 88 (1968)
29. T. Kawai and T. Kuriyama, *Sen-i Gakkaishi (in Japanese)* 1-5 (1964)
30. P. J. Flory, *Trans Faraday Soc*. **57**, 829 (1961)
31. R. J. Roe and W. R. Krigbaum, *J. Polym. Sci*. **61**, 167 (1962)
32. T. Asano and Y. Fujiwara, *Polymer,* **19**, 99 (1978)
33. T. Asano, *Reports of Fac, Sci. Shizuoka Univ.*, **6**, 17, (1971)
34. T. Asano, Y. Fujiwara and T. Yoshida, *Polym. J.*, **11**, 383-390 (1979)
35. T. Yoshida, Y. Fujiwara and T. Asano, *Polymer*, **24**, 925-929 (1983)